# Physica Scripta



RECEIVED 25 April 2025

REVISED 3 July 2025

ACCEPTED FOR PUBLICATION

ACCEPTED FOR PUBLICATION 17 July 2025

PUBLISHED 30 July 2025

#### **PAPER**

# Secondary shearless bifurcations in tokamaks

Bruno Borges Leal\* , Lucas Nedeff Assub Amaral and Iberê Luiz Caldas

Institute of Physics, University of São Paulo, 05508-900, São Paulo, SP, Brazil

\* Author to whom any correspondence should be addressed.

E-mail: bruno.borges.leal@alumni.usp.br

Keywords: secondary shearless curve, magnetic field line, transport, isochronous island chain, tokamak, symplectic map

#### **Abstract**

Isochronous island chains have been shown to have an impact on plasma transport. To investigate this effect, we use an area-preserving twist map that describes the trajectories of the magnetic field lines in a tokamak with an ergodic limiter composed of two pairs of coils. In this setup, the plasma is perturbed by two independent modes that act on the same magnetic surface, which provides a framework for analyzing scenarios where isochronous bifurcations occur. These bifurcations are associated with the emergence of secondary shearless curves, which, like shearless curves in nontwist systems, act as robust transport barriers, but locally, restricting the transport of chaotic field lines in the regions near the island chains. By computing the internal rotation number, we identify the presence of secondary shearless curves and analyze their dependence on the perturbation parameters. We show that these curves may emerge, persist, or break as the parameters vary, and that even after breaking, they continue partially restricting field line transport. This persisting trapping effect might serve as a possible explanation of the results observed in previous works.

## 1. Introduction

It is widely known that the trajectories of the magnetic field lines in a tokamak follow a Hamiltonian structure [1–3]. The toroidal and poloidal fields of the plasma equilibrium correspond to an integrable Hamiltonian system, while external magnetic perturbations can be described by a perturbation in the Hamiltonian, making the system quasi-integrable [4]. As a result, it exhibits phenomena characteristic of quasi-integrable Hamiltonian systems [5, 6], such as the coexistence of regular and chaotic orbits, the formation of island chains, and the progressive destruction of KAM tori.

This enables the use of Hamiltonian models for field line trajectories to study certain plasma phenomena. Although the assumption that plasma particles strictly follow field line orbits is a first-order approximation—so that particle dynamics may differ substantially [7-10]—these models still offer valuable insight into the physical processes occurring in tokamaks and have been widely used to analyze general dynamical properties [11-14].

A key feature of quasi-integrable Hamiltonian systems is the presence of isochronous island chains—better known in plasma physics as heteroclinic islands. By definition, these are independent island chains that arise from different initial conditions, share the same winding number, and are generated by perturbation modes acting on the same KAM torus [15, 16]. This phenomenon is a topic of interest in various fields, such as atomic and molecular physics [17], solid-state physics [18], particle acceleration [15], and nonlinear dynamics [19].

In plasma physics, recent studies have shown the formation of isochronous island chains in the plasma due to bifurcations. In MHD simulations of the NSTX-U tokamak equipped with nonaxisymmetric control coils (NCCs), bifurcations in the island chains led to the emergence of isochronous islands [20]. Furthermore, an experimental investigation in DIII-D has also shown bifurcations giving rise to isochronous island chains [21]. This topic is highly relevant because isochronous island chains can significantly impact plasma confinement. Reference [20] showed that, under certain plasma conditions, they can enhance confinement, while [21] indicated that they may reduce the efficiency of mechanisms designed to prevent disruptions in the plasma column.

Motivated by these works, a model was proposed to investigate isochronous bifurcations in tokamaks [22]. This model is a symplectic map that describes the magnetic field of a tokamak equipped with an ergodic limiter with two pairs of coils. These coils generate two independent modes,  $(m_1, n_1)$  and  $(m_2, n_2)$ , allowing for the exploration of various bifurcation configurations. The results indicated that these bifurcations can lead to the formation of secondary shearless curves.

To understand these curves, it is important to first define twist and nontwist systems. Dynamical systems are classified as *twist* if the rotation number (which, in a tokamak, corresponds to the inverse of the safety factor) is monotonic, and as *nontwist* if there is a region in phase space where the derivative of the rotation number vanishes [12, 23–25]. Tokamak magnetic fields, which typically have a monotonic safety factor, are thus classified as twist systems. In the Poincaré section of nontwist systems, the region where the derivative vanishes is called the *shearless curve*, which acts as a robust transport barrier. Twist systems do not contain such curves, however, they can exhibit secondary (or internal) shearless curves, which also serve as transport barriers [26–28]. Transport barriers associated with non-monotonic profiles are also observed in particle dynamics models, where regions near extrema of the q-kinetic profile inhibit transport [29, 30]. In the present work, however, we restrict our analysis to field line dynamics.

A recent study using the same model as reference [22], but employing the cylindrical approach, showed that isochronous bifurcations are usually accompanied by the emergence of secondary shearless curves [31]. In the present work, we use a variation of the previous model that incorporates the toroidicity of the tokamak to show that these results also apply in this more realistic scenario.

In section 2, we introduce the new model. Section 3 defines secondary shearless curves and explains how they are characterized by the internal rotation number [5, 6]. In section 4, we present the results obtained with the map, where we observe the emergence and breaking of secondary shearless curves. Additionally, we analyze a permitvity diagram that illustrates how field line transport is influenced by isochronous islands.

### 2. The model

We consider a tokamak equipped with an ergodic limiter formed by a set of pairs of coils with length g much smaller than  $2\pi R_0$ , where  $R_0$  is the major radius of the tokamak. Each coil in a pair is toroidally positioned  $\pi$  radians from its counterpart, and each coil has a toroidal displacement of  $\Delta \phi = 2\pi/N$  radians from its nearest neighbor, where N is the total number of coils. A pair of these coils can excite a mode with a defined toroidal and poloidal wave number, denoted by m and n, which resonates with the rational surface at q = m/n, creating magnetic island chains. In this work, we investigate the effects of the coupling of resonant modes by considering an ergodic limiter with two pairs of coils generating two modes,  $(m_1, n_1)$  and  $(m_2, n_2)$ . In this case N = 4 and  $\Delta \phi = \pi/2$ .

As mentioned before, the trajectories of the magnetic field lines in a tokamak are described by a Hamiltonian system. Therefore, the evolution of the field lines around the torus can be modeled by an area-preserving map, which retains the same Hamiltonian structure. This map provides the points of intersection of the field lines with a transversal surface crossing the tokamak chamber, called the Poincaré section. We used this technique to study the dynamics of magnetic field lines in a tokamak with an ergodic limiter consisting of two pairs of coils. Figure 1 illustrates the configuration.

To exemplify this, we analyze a Poincaré section of the Ullmann map, which describes a tokamak with an ergodic limiter consisting of a single pair of coils, which corresponds to the model presented in figure 1 with the pair of coils  $(2_1, 2_2)$  turned off. We consider a plasma with q(a) = 5 and a perturbation mode (5, 1). Figure 1(a) shows the resulting Poincaré section in Cartesian coordinates. The perturbation primarily affects the rational surface at q = 5/1, creating an island chain with period 5 and creating chaos near the plasma edge. Smaller secondary islands also emerge. Figure 2(b) presents the same section but in terms of normalized polar coordinates,  $X = \theta/2\pi$  and Y = (b-r)/b, where b is the radius of the plasma column. While this representation is less visually intuitive, it is far more common in the study of dynamical systems and will be used throughout the remainder of this paper.

The map used to obtain the results in this work is a variation of the Ullmann map [32] that incorporates the effect of two pairs of coils, each spaced by  $\Delta\phi=\pi$ . It consists of two parts: the first describes the evolution of field lines in the absence of magnetic perturbations, while the second accounts for the perturbation caused by the limiter coils. In the unperturbed case, the field line position  $(r^*, \theta^*)$  is mapped from its previous position  $(r, \theta)$  according to:

$$r^* = \frac{r}{1 - \frac{1}{N} a_1 \sin \theta},\tag{1}$$

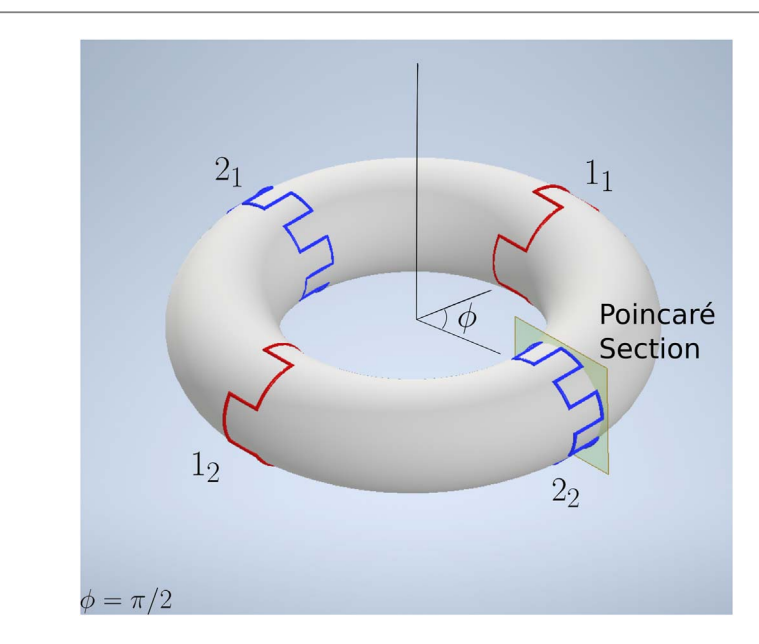
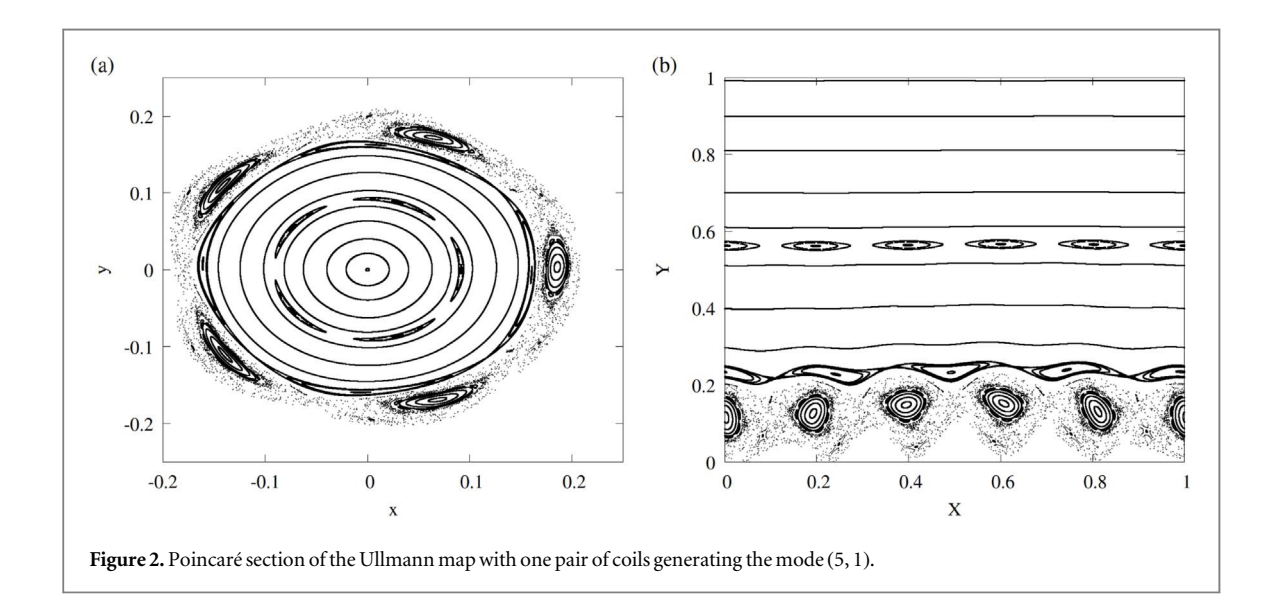


**Figure 1.** Schematic figure showing the coil setting and a representation of the Poincaré section. Here,  $i_k$  denotes the ith pair of coils, where i = 1, 2 labels the pair, and k = 1, 2 distinguishes the first and second coil within each pair.



$$\theta^* = \theta + \frac{1}{N} \frac{2\pi}{q(r^*)} + \frac{1}{N} a_1 \cos \theta, \tag{2}$$

where N = 4 is the number of coils, q(r) is the safety factor, and  $a_1$  is a parameter accounting for the toroidicity of the field lines. These expressions are derived from a generating function in which the toroidal correction appears as a series expansion [32]. Neglecting all terms in this series yields the cylindrical approximation, as used in [31]. In the present work, we retain the first-order term of the series and consider the parameters of the TCABR tokamak [33], which yields  $a_1 = -0.02$ .

For the perturbed part, the position of the field line immediately after passing through a coil is given by:

$$r^* = r + \frac{bm_i C_i}{m_i - 1} \left(\frac{r}{b}\right)^{m_i - 1} \sin[m_i(\theta^* + (k - 1)\alpha_i)],\tag{3}$$

$$\theta = \theta^* - C_i \left(\frac{r}{b}\right)^{m_i - 2} \cos[m_i(\theta^* + (k - 1)\alpha_i)]. \tag{4}$$

In this expression, b is the minor radius of the tokamak and the perturbation is characterized by the toroidal and poloidal mode numbers  $m_i$  and  $n_i$  of the pair of coils i = 1, 2, which define the phase factor  $\alpha_i = \pi n_i/m_i$ . Physically, this phase is the relative poloidal angle between coils of the same pair. The index k = 1, 2 distinguishes the two coils of the i-th pair. The perturbation strength is given by the dimensionless parameter

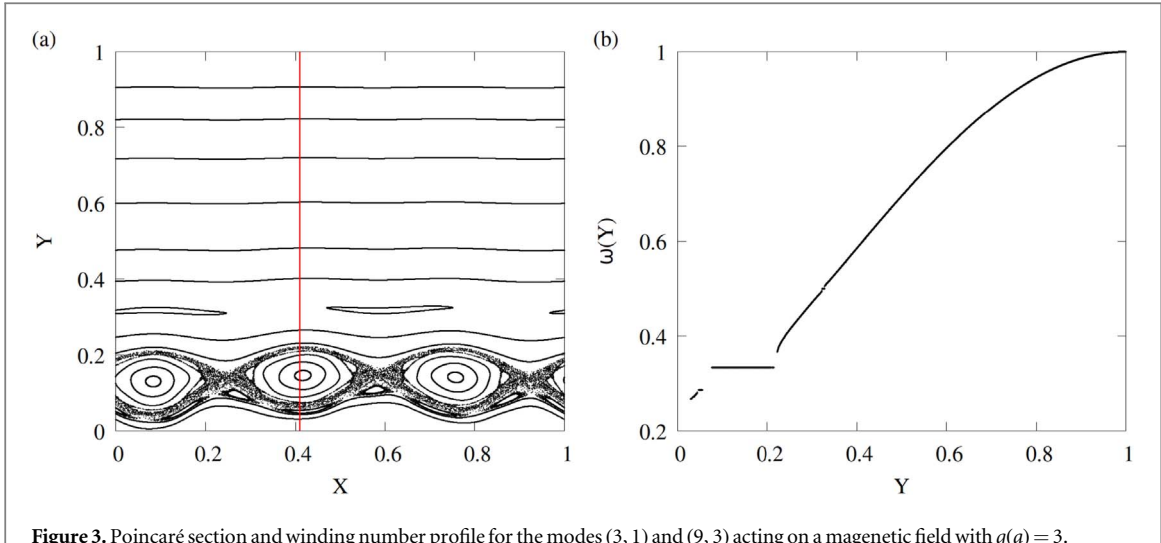


**Figure 3.** Poincaré section and winding number profile for the modes (3, 1) and (9, 3) acting on a magenetic field with q(a) = 3.

$$C_i = \frac{2\epsilon_i m_i g a^2}{a(a)Rb^2},\tag{5}$$

where  $\epsilon = I_l/I_p$  is the ratio of the perturbation coil current to the plasma current, R is the tokamak's major radius, and a is the plasma column radius. The parameter q(a) represents the safety factor at r = a while g, as mentioned before, is the length of each coil.

Using this set of equations, we can track the trajectory of the field lines by choosing an initial condition and applying equations (3) and (4) when the field line passes through a coil, and equations (1) and (2) to follow its path between coils. Since there are four coils, starting from an initial condition in the Poincaré section, we apply each of the maps four times to determine the next intersection with the section. Figure 3(a) shows a Poincaré section of the resulting map for the modes (3, 1) and (9, 3) with a safety factor profile with q(a) = 3. In this case, the amplitudes of the perturbations are such that the primary mode (3, 1) dominates, forming a single chain of three islands near the plasma edge.

# 3. Secondary shearless curves

The safety factor is an important parameter in tokamak operation and has a direct correspondence with the field line winding number  $\omega$ , which is widely used in dynamical systems analysis:

$$q = \frac{1}{\omega} \tag{6}$$

The winding number has a clear physical meaning for our system. It determines the average poloidal displacement of a field line, on a magnetic surface, per toroidal turn. If  $\omega$  is a rational number ( $\omega = r/s$ ), the field line is closed, as it returns to the exact same position after s turns around the torus. On the other hand, if  $\omega$  is irrational, the field line never closes and instead densely covers the corresponding toroidal magnetic surface. The winding number is not defined for chaotic orbits.

From a numerical standpoint, the winding number for a magnetic field line crossing the Poincaré section at  $(r_0, \theta_0)$  at the mapping iteration l = 0 is calculated by:

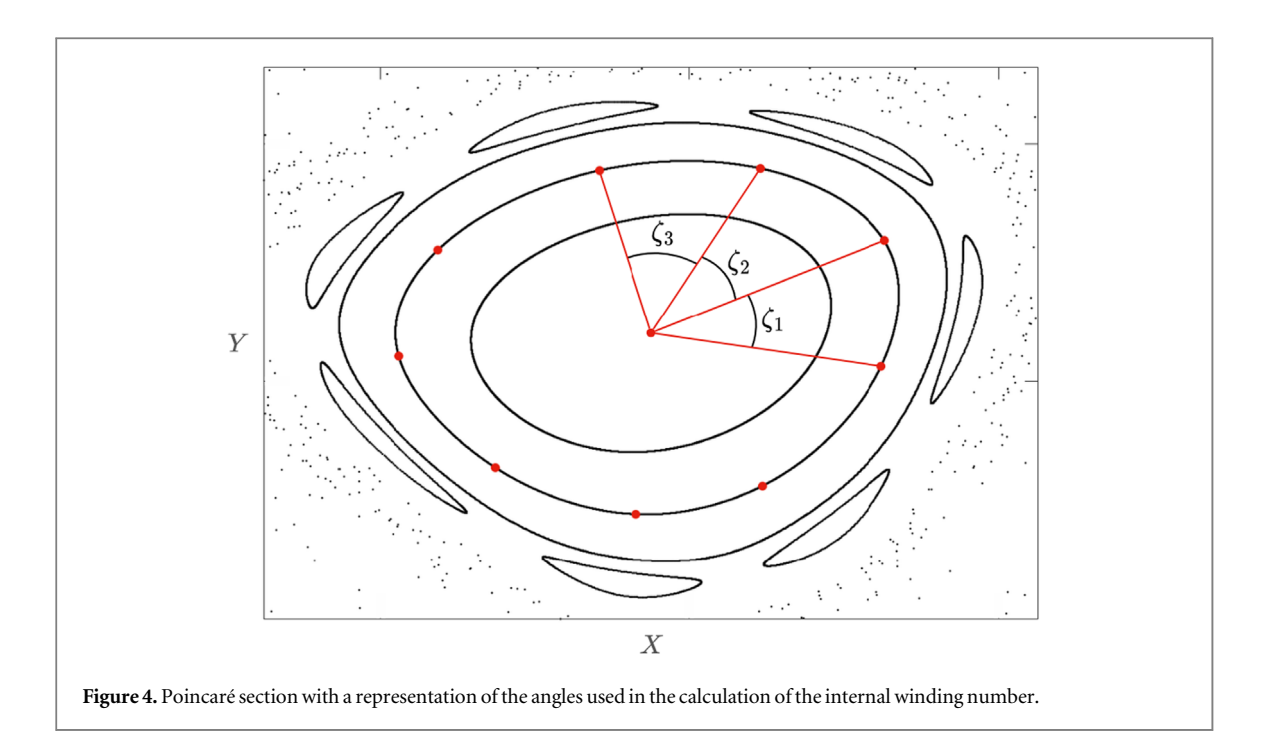
$$\omega = \lim_{k \to \infty} \frac{1}{2\pi k} \sum_{l=0}^{k} (\theta_{l+1} - \theta_l). \tag{7}$$

Figure 3(b) shows the winding number profile calculated along a line of constant X in the section shown in figure 3(a). If the equilibrium winding number profile with respect to Y is monotonic, like in this example, the system is called a twist system, since it satisfies the twist condition:

$$\frac{\mathrm{d}\omega}{\mathrm{d}Y} \neq 0,\tag{8}$$

at every point in phase space.

Thus, tokamaks with a monotonic safety factor profile are twist systems. Conversely, if the profile has an extremum, where  $d\omega/dY = 0$ , the system is called nontwist. In such cases, the solution that violates the twist condition corresponds to an invariant curve known as the shearless (or twistless) curve.



In both twist and nontwist systems, invariant curves act as transport barriers, restricting chaotic orbits from accessing certain regions of phase space. In twist systems, as the perturbation increases, these barriers are progressively destroyed, as dictated by the KAM theorem. However, the KAM theorem does not apply to nontwist systems. In such cases, the shearless curve persists even under strong perturbations, making it a robust transport barrier.

By definition, in twist systems, the derivative of the winding number never vanishes, and shearless curves do not exist. However, a local winding number can be defined to describe the rotation of an island around its elliptical point. This quantity, known as the internal winding number, is calculated by:

$$\omega_{\rm in} = \lim_{k \to \infty} \frac{1}{2\pi k} \sum_{l=0}^{k} (\zeta_{l+1} - \zeta_l) \tag{9}$$

where  $\zeta$  represents the angle between consecutive points in the island, as shown in figure 4. Even in twist systems, the internal winding number profile can be non-monotonic. In such cases, the curves corresponding to the extreme points in the profile are called secondary shearless curves [27]. In the following section, we investigate the emergence of secondary shearless curves in the system presented in the previous section, regarding a tokamak with two pairs of limiter coils.

# 4. Results

We consider the case in which the first pair of coils generates the mode (3, 1) and the second generates the mode (9, 3). The amplitude of the first perturbation is kept constant, while the amplitude of the second is gradually increased. The initial scenario is shown in figure 5(a), where we observe the presence of a secondary shearless curve (in red) that emerges due to the coupling of the resonant modes. This shearless curve divides the phase space into two regions, both containing chaotic orbits; however, the chaotic trajectories enclosed by the shearless curve cannot escape to the outer region, and vice versa.

Figure 6(a) shows a magnified view of the same section, where a pair of (26, 3) twin islands (highlighted in blue and green) are seen above and below the shearless curve. Figure 6(b) displays the internal winding number profile computed along a line crossing the shearless curve (indicated in purple in figure 6(a)). The shearless curve corresponds to a local maximum in the winding number profile, while the twin island chains are associated with the plateaus at  $\omega = 3/26$ .

As the amplitude of the second mode increases, the secondary shearless curve eventually breaks (figure 5(b)) and later reappears (figure 5(c)). In the latter case, we again identify the shearless curve by the local maximum in the winding number profile (figure 6(d)). A pair of (117, 4) twin islands, highlighted in blue and green in figure 6(c), is also observed.

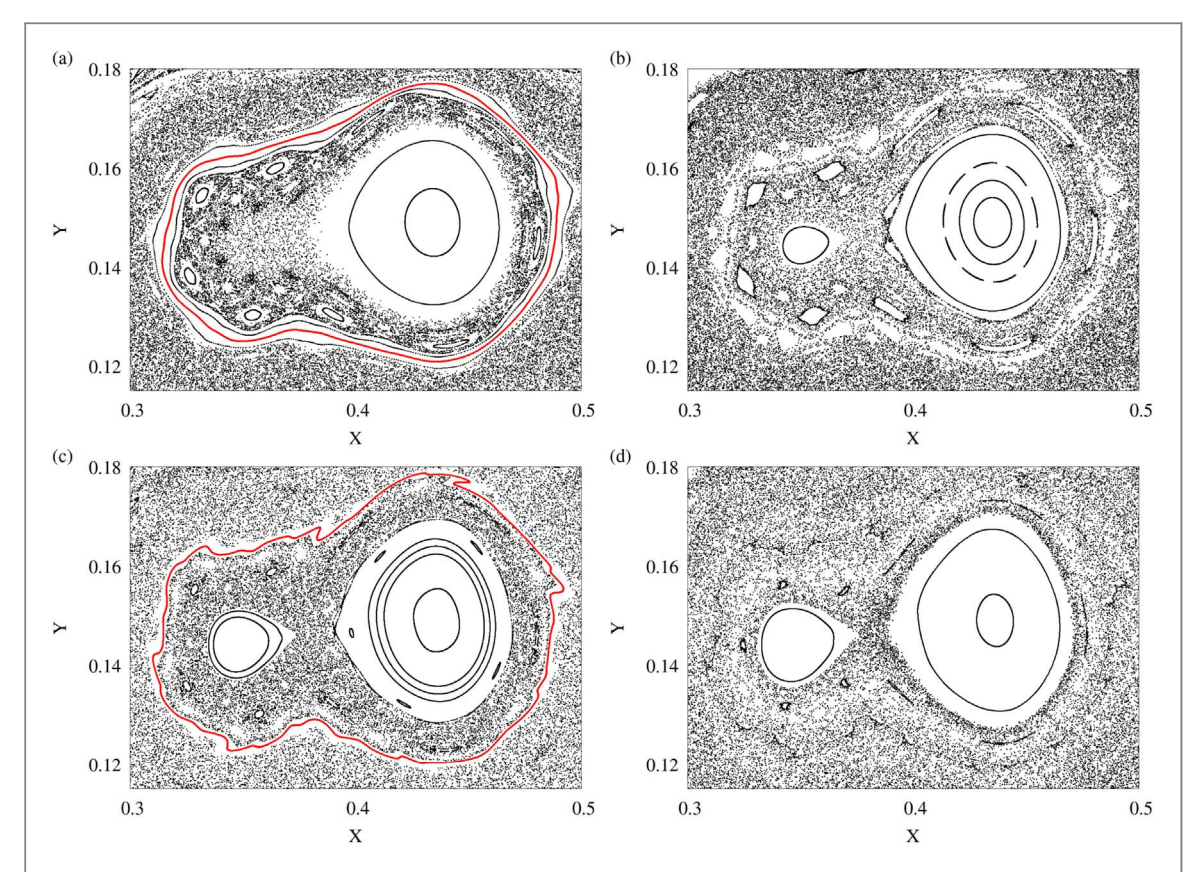


**Figure 5.** An example of the breaking and resurgence of the secondary shearless curve as  $\epsilon_2$  increases. In (a), for  $\epsilon_2=1.0731\times 10^{-2}$ , the internal shearless curve is present. Then the curve disappears, as shown in (b) for  $\epsilon_2=1.2525\times 10^{-2}$ , and reappears again, as shown in (c) for  $\epsilon_2=1.4120\times 10^{-2}$ . In (d), for  $\epsilon_2=1.5003\times 10^{-2}$ , it has disappeared once more. For all cases,  $\epsilon_1=1.1296\times 10^{-2}$ .

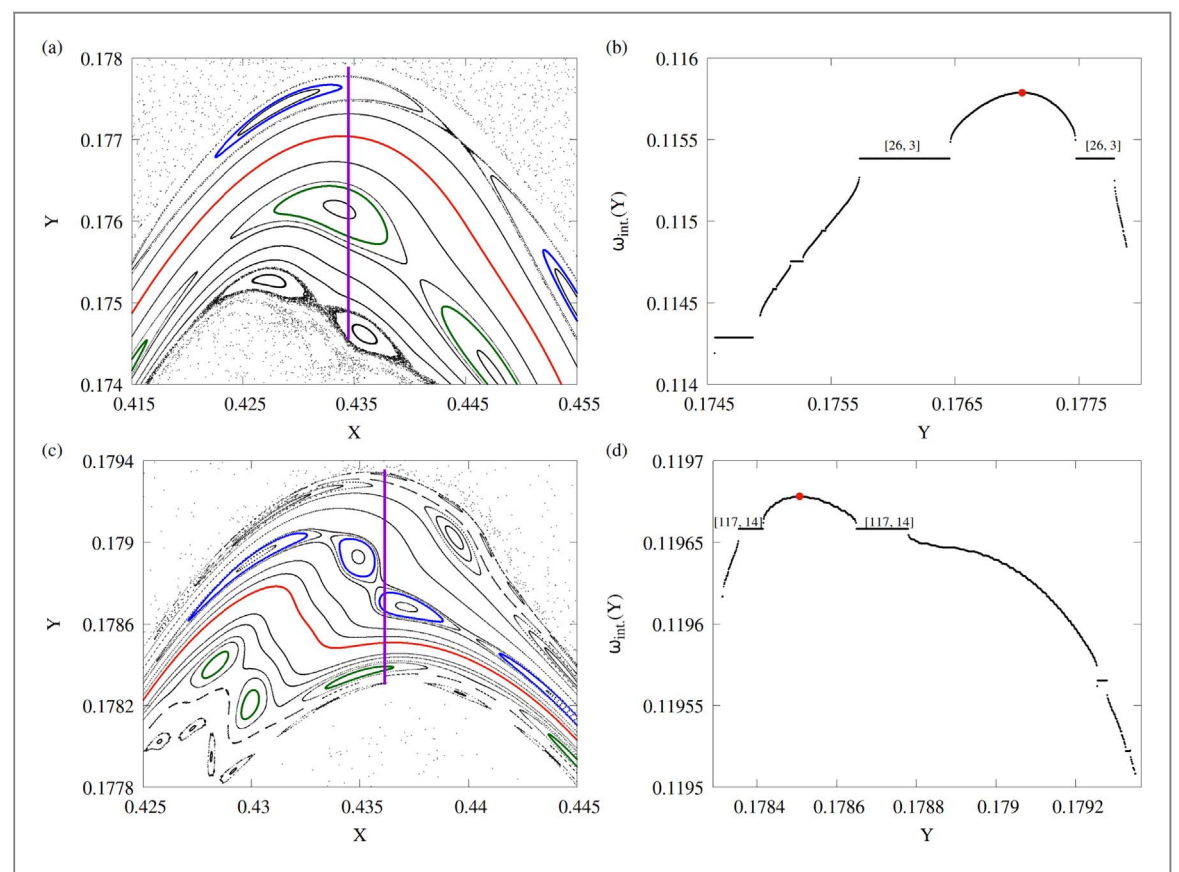
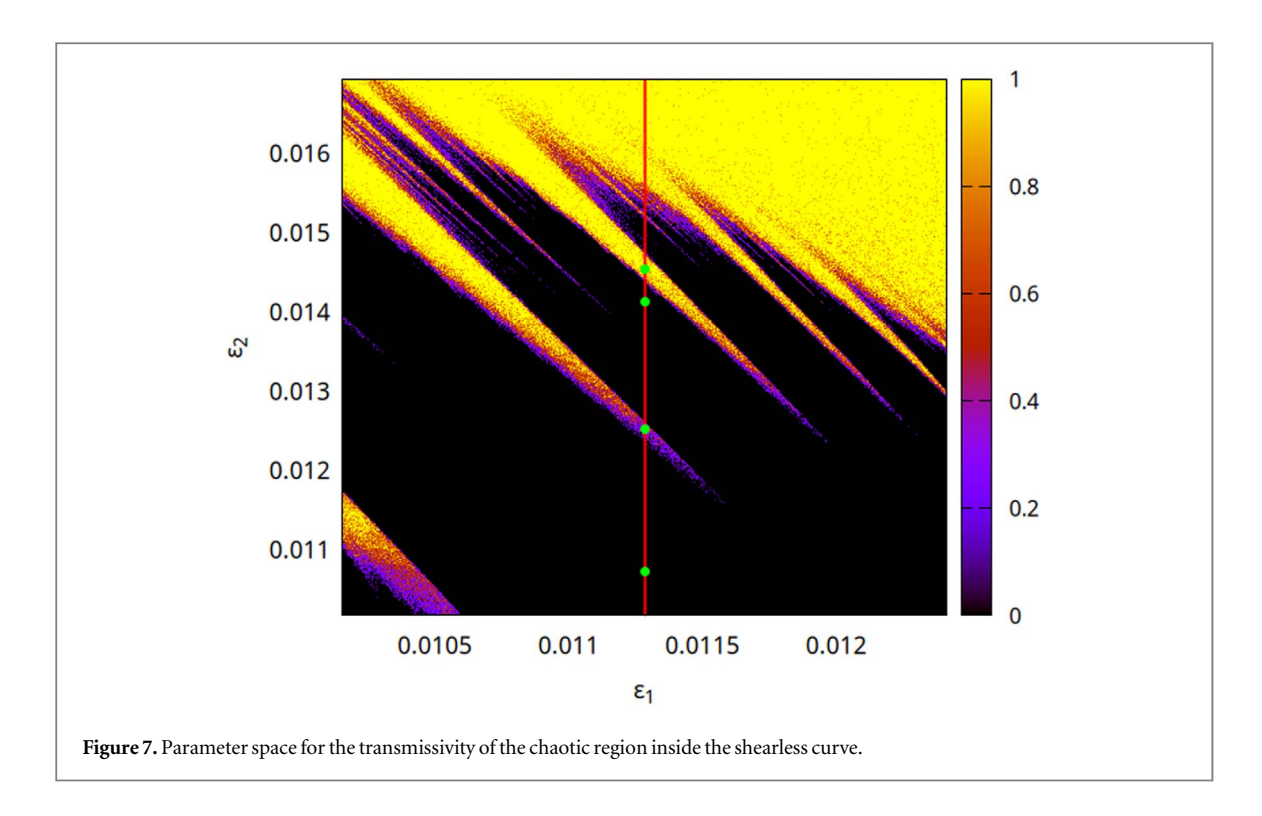


Figure 6. Amplifications of the Poincaré sections in figures 5(a) and 5(c) and the corresponding winding number profiles.



Finally, in the last example, the shearless curve is destroyed once more, as shown in figure 5(d). The breaking and resurgence of shearless curves, as well as the appearance of twin islands, which are behaviors typical of non-twist systems, occur locally, despite the system being globally twist.

To assess how the perturbation parameters and the presence of secondary shearless curves influence transport, we select an ensemble of initial conditions within the chaotic region enclosed by the shearless curve and compute their transmissivity, which corresponds to the fraction of orbits that escape this region within a given number of iterations [34]. For this calculation, we use a maximum of  $6 \times 10^4$  iterations. This quantity is evaluated for various values of  $\epsilon_1$  and  $\epsilon_2$ , which denote the perturbation strengths of each mode. The results are shown in the parameter space of figure 7.

The four green dots indicate the parameter values corresponding to the previously analyzed sections. In the first case, the transmissivity is zero, showing that the secondary shearless curve functions as a completely impermeable transport barrier. In the second case, the curve is broken, permitting limited transport. In the third case, the shearless curve resurges, once again fully inhibiting transport. Finally, in the last scenario, no transport barrier exists, and the transmissivity is very high.

An important aspect revealed by this result is that, even after the curve is broken, it continues to act as a partial transport barrier. This persistent trapping effect may account for the accumulation of chaotic field lines around the magnetic islands of heteroclinic chains observed in [20].

It would be possible to identify the perturbation configurations that lead to the formation of internal shearless curves by constructing a parameter space similar to that of figure 7, but indicating, for each pair of values for  $\epsilon_1$  and  $\epsilon_2$ , the presence or absense of the shaerless curve, instead of the transmissivity.

#### 5. Conclusion

We used a symplectic map to describe the intersection of magnetic field lines with a plane transverse to the tokamak toroidal chamber, defining our Poincaré section. The magnetic field lines were periodically perturbed in space by the magnetic coils that make up the magnetic ergodic limiter, the device responsible for generating resonances and creating chaos at the plasma edge.

We considered an ergodic limiter configuration so that the magnetic field is perturbed by two different modes acting on the same magnetic surface. As a result, we observed the emergence of local shearless curves, which were identified by the internal winding number profiles. We observed that internal shearless curves act as local transport barriers, trapping chaotic magnetic field lines near the resonance region created by the perturbation modes. These curves are robust, meaning they persist as the perturbation increases and continue to inhibit transport even after being broken, as evidenced by the reduced transmissivity in those cases.

We also showed that as the perturbation amplitude increases, secondary shearless curves can reappear after being broken. This phenomenon is typical of nontwist systems, where it occurs globally in the Poincaré section. We concluded that the same phenomenon occurs locally in twist systems, specifically around the elliptic points.

Finally, we showed that the trapping effect associated with internal shearless curves persists even after they break, and we propose that this effect may explain the results observed in [20].

# Acknowledgments

This research was supported by the Fundação de Amparo à Pesquisa do Estado de São Paulo (FAPESP) under Grant Nos. 2024/05700-5 and 2022/15489-4, and the Conselho Nacional de Desenvolvimento Científico e Tecnológico (CNPq) under Grant Nos. 302665/2017-0 and 200428/2025-0.

# Data availability statement

All data that support the findings of this study are included within the article (and any supplementary files).

### References

- [1] Cary J R and Littlejohn R G 1983 Noncanonical hamiltonian mechanics and its application to magnetic field line flow Ann. Phys., NY 1511
- [2] Boozer A H 2004 Physics of magnetically confined plasmas Rev. Mod. Phys. 76 1071
- [3] Viana R L, Mugnaine M and Caldas I L 2023 Hamiltonian description for magnetic field lines in fusion plasmas: A tutorial *Phys. Plasmas* 30 090901
- [4] Lichtenberg A J and Lieberman M A 2013 Regular and Chaotic Dynamics vol 38 (Springer Science & Business Media)
- [5] Meiss J D 1992 Symplectic maps, variational principles, and transport Rev. Mod. Phys. 64 795
- [6] Ott E 2002 Chaos in Dynamical Systems (Cambridge University Press)
- [7] Cambon B et al 2014 Chaotic motion of charged particles in toroidal magnetic configurations Chaos 24 033101
- [8] Ogawa S et al 2016 Full particle orbit effects in regular and stochastic magnetic fields Phys. Plasmas 23 072506
- [9] Moges HT et al 2024 Kinetic vs magnetic chaos in toroidal plasmas: A systematic quantitative comparison Phys. Plasmas 31 012302
- [10] Wingen A et al 2006 Influence of stochastic magnetic fields on relativistic electrons Nucl. Fusion 46 941
- [11] Balescu R, Vlad M and Spineanu F 1998 Tokamap: A hamiltonian twist map for magnetic field lines in a toroidal geometry Phys. Rev. E 58 951
- [12] Morrison PJ 2000 Magnetic field lines, hamiltonian dynamics, and nontwist systems Phys. Plasmas 7 2279
- [13] Martins C G L, Roberto M and Caldas I L 2014 Delineating the magnetic field line escape pattern and stickiness in a poloidally diverted tokamak Phys. Plasmas 21 082506
- [14] Abdullaev S S et al 2006 Mappings of stochastic field lines in poloidal divertor tokamaks Nucl. Fusion 46 S113
- $[15] \ de Sousa \ MC\ et\ al\ 2013\ Alternate\ islands\ of\ multiple\ isochronous\ chains\ in\ wave-particle\ interactions\ Phys.\ Rev.\ E\ 88\ 064901$
- [16] Evans T E et al 2021 Observations of heteroclinic bifurcations in resistive magnetohydrodynamic simulations of the plasma response to resonant magnetic perturbations *Phys. Rev. E* 103 013209
- $[17] \ Conforti \ Met \ al \ 2016 \ Heteroclinic \ structure \ of \ parametric \ resonance \ in \ the \ nonlinear \ schrödinger \ equation \ Phys. \ Rev. \ Lett. \ 117\ 013901$
- [18] Lei Y and Fu R 2016 Heteroclinic chaos in a josephson-junction system perturbed by dichotomous noise excitation Europhys. Lett. 112 60005
- [19] Mugnaine M et al 2024 Isochronous bifurcations in a two-parameter twist map Phys. Rev. E 110 024206
- [20] Wu W et al 2019 Topological bifurcation of magnetic islands in NSTX-U Nucl. Fusion 59 066010
- [21] Bardóczi L and Evans T E 2021 Experimental observation of magnetic island heteroclinic bifurcation in tokamaks *Phys. Rev. Lett.* 126 085003
- [22] Leal B B et al 2024 Isochronous island bifurcations driven by resonant magnetic perturbations in tokamaks Phys. Rev. E 109 014230
- [23] del Castillo-Negrete D and Morrison P J 1993 Chaotic transport by rossby waves in shear flow Physics of Fluids A: Fluid Dynamics 5 948
- [24] del Castillo-Negrete D, Greene J M and Morrison P J 1996 Area preserving nontwist maps: periodic orbits and transition to chaos Physica D 91 1
- [25] Grime G C et al 2023 Caldas. Shearless curve breakup in the biquadratic nontwist map Chaos, Solitons Fractals 172 113606
- [26] Dullin H R, Meiss J D and Sterling D 2000 Generic twistless bifurcations Nonlinearity 13 203
- [27] Abud CV and Caldas IL 2012 Secondary nontwist phenomena in area-preserving maps Chaos 22
- [28] Abud CV and Caldas IL 2014 Onset of shearless magnetic surfaces in tokamaks Nucl. Fusion 54 064010
- [29] Anastassiou G et al 2024 Role of the edge electric field in the resonant mode-particle interactions and the formation of transport barriers in toroidal plasmas I. Plasma Phys. 90 905900110
- [30] Shinohara K et al 2018 Estimation of orbit island width from static magnetic island width, using safety factor and orbit pitch Nucl. Fusion 58 082026
- [31] Leal B B et al 2025 Secondary shearless bifurcations for two isochronous resonant perturbations Chaos 35 043136
- [32] Ullmann K and Caldas I L 2000 A symplectic mapping for the ergodic magnetic limiter and its dynamical analysis *Chaos, Solitons Fractals* 11 2129
- [33] da Silva E C, Caldas I L and Viana R L 2002 Ergodic magnetic limiter for the tcabr Braz. J. Phys. 32 39
- [34] Szezech J D Jr. et al 2009 Transport properties in nontwist area-preserving maps Chaos 19 043108